Crystal Growth Mechanism Changes in Pseudo-Dewetted Poly(ethylene oxide) Thin Layers

Dun-Shen Zhu,[†] Yi-Xin Liu,[†] Er-Qiang Chen,*[,†] Ming Li,[‡] Chao Chen,[†] You-Hai Sun,[†] An-Chang Shi,*[,§] Ryan M. Van Horn,[⊥] and Stephen Z. D. Cheng[⊥]*[,†,]

Department of Polymer Science and Engineering and Key Laboratory of Polymer Chemistry and Physics of Ministry of Education, College of Chemistry and Molecular Engineering, Peking University, Beijing 100871, China; Institute of Physics, CAS, Beijing 100080, China; Department of Physic and Astronomy, McMaster University, Hamilton, Ontario L8S 4M1, Canada; and Maurice Morton Institute and Department of Polymer Science, The University of Akron, Akron, Ohio 44325-3909

Received November 3, 2006; Revised Manuscript Received January 10, 2007

ABSTRACT: Changes in the crystal growth mechanism were observed in pseudo-dewetted, thin layers of low molecular weight (MW) poly(ethylene oxide) (PEO) on a hydrophilic mica surface. The studies were conducted using two PEO fractions (HPEO and MHPEO) with similar MW's (number-average MW of around 4500 g/mol) but different end-group chemistries. For the HPEO, both ends of the chain are capped by −OH groups. For the MHPEO, one end is capped by an −OH group, while the other end is capped by an $-OCH_3$ group. Utilizing in-situ atomic force microscopy, the growth of single crystals as a function of time (t) was monitored at different crystallization temperatures (T_x). Depending on the end-group chemistry and T_x applied, two growth laws were observed, which state that the crystal lateral size r or the crystal volume V can be linearly proportional to t ($r \propto t$ or $V \propto t$). Combined with morphological observations of the single crystals, it could be deduced that when $r \propto t$, the crystal growth was nucleation-limited (NL), while in the case of $V \propto t$, and thus $r \propto t^{0.5}$ at constant crystal thickness, the crystal growth was diffusion-limited (DL). A change of the crystal growth mechanism from the NL to the DL process was also observed with decreasing T_x in the MHPEO sample.

Introduction

For a polymer system in a metastable state, such as a supercooled liquid at a given supercooling (ΔT), a newly formed stable phase (such as a crystal phase) can be dispersed in the metastable phase. This two-phase coexistence is not at thermodynamic equilibrium. The total free energy of the system can be decreased by growing the stable (crystal) phase and reducing the crystal/liquid interfaces. The kinetics of crystal growth is usually governed by one of two processes: a mass transport process via diffusion or a nucleation process via molecular attachment and detachment. Depending on the thermodynamics and conditions of crystal growth, the limiting factor can be either diffusion or nucleation.[1−8] Namely, when the slowest step in a crystal growth is the nucleation process, this crystal growth is nucleation-limited (NL). On the other hand, if the slowest step in a crystal growth is the diffusion process, the crystal growth is then diffusion-limited (DL). In polymers, when a system is reduced from three-dimensional (3D) to quasi-two-dimensional (2D) space, as realized in thin films with the thickness comparable to the radius of gyration (R_g) of polymer chains (usually several to tens of nanometers), the behavior of polymer crystallization is qualitatively changed.[9,10] For example, the thin layer can anisotropically suppress the polymer density fluctuation so that the crystal growth may be altered as compared with that of bulk (3D) crystallization. Therefore, interesting questions arise: when a monolayer single crystal sets in the thin melt layer with a thickness of a few to tens of nanometers, what is the limiting factor for the crystal growth? How much suppression on the crystal growth rate can be achieved due to the growth from the quasi-2D thin layer of the polymer melt?

In the past decade, many studies have been focused on the polymer crystallization from thin layers on solid substrates. As an example, it has been observed that varying the ΔT and the layer thickness in isotactic polystyrene (*i*-PS) leads to various crystal morphologies including faceted single crystals, a compact seaweed, dense branching morphology, or fractal dendrites.[11−13] At very low ΔT and relatively thick layers, the *i*-PS faceted monolayer single crystals grow with a linear growth rate, indicating clearly a NL growth mechanism. On the other hand, the branching morphologies, which are usually formed at relatively high ΔT values, are believed to be associated with the existence of a diffusion field within the thin layers. The growth of the branching tips is measured to be a linear function of crystallization time, but the growth rate is significantly slower than those found in *i*-PS bulk crystallization. Moreover, at the same crystallization temperature (T_x), the growth rate is decreased with decreasing layer thickness, until the layer thickness approaches the lamellar thickness. These previous studies on *i*-PS have provided remarkable results including quantitative data for crystallization kinetics and morphological instability of thin layer polymer crystallization. Another polymer chosen as a model compound for thin layer crystallization is poly(ethylene oxide) (PEO) fractions.[14−25] Similar to those observed in *i*-PS, the growth rate of the PEO crystals is decreased with the layer thickness, and different morphologies have been obtained by varying T_x. A theoretical model analogous to diffusion-limited aggregation (DLA) has been proposed to describe the formation of polymer fractal dendrites.[14,16]

However, understanding of the polymer crystal growth in thin layers is still far from complete. In this publication, we describe our efforts on investigation of the kinetic mechanisms of polymer single crystals grown from the thin layer melt on a

* To whom correspondence should be addressed. E-mail: eqchen@pku.edu.cn, shi@mcmaster.ca, and scheng@uakron.edu.
[†] Peking University.
[‡] Institute of Physics, CAS.
[§] McMaster University.
[⊥] The University of Akron.

10.1021/ma062542s CCC: $37.00 © 2007 American Chemical Society
Published on Web 02/10/2007

hydrophilic mica surface using two low molecular weight (MW) PEO fractions with different end-group chemistries. One of the samples, which will be referred to as HPEO, has an −OH at both chain ends, and the other, MHPEO, has one end of $-OCH_3$ and another one of −OH. It is well-known that the low-MW PEO fractions can form lamellar crystals with the lamellar thickness (L) to be the integral fraction of the chain length [IF(n)],[26−30] in which $L = l_u N/(n+1)$, with $l_u = 0.278$ nm, N is degree of polymerization, and n is the fold number ($n = 0$, 1, 2, ...). These IF(n) crystals can also form in the PEO thin layers. They are usually monolayer flat-on lamellae on the hydrophilic solid substrates.[14−18,21−24]

Thin layers of PEO can be obtained by either spin-coating or static casting from solution. After the thin layer on a hydrophilic substrate is heated above the melting temperature (T_m) of PEO crystals, a pseudo-dewetting melt structure will usually be formed. Namely, the strong interaction between the −OH end groups of PEO molecules and the substrate surface favors an adsorbed (wetted) thin monolayer with a thickness of 4−6 nm, and the nonadsorbed PEO molecules form droplets sitting on the top of the monolayer presumably due to autophobic dewetting.[14,15,31,32] This pseudo-dewetted melt structure can be retained in supercooled conditions. When the crystal growth takes place from the pseudo-dewetted thin layers, the newly formed IF(n) crystals with fixed lamellar thickness can be unambiguously distinguished from the melt by using the atomic force microscopy (AFM) technique. Therefore, we utilize in-situ AFM to follow the crystal growth process and their morphological evolution when the PEO single crystals grow from the pseudo-dewetted thin layer melt. Our observations reveal, for the first time, a ΔT and chain end-group chemistry dependence of the growth mechanism. A crossover from an NL process to a DL process can also be found.

Experimental Section

Materials and Sample Preparation. The samples of HPEO and MHPEO were purchased from Polymer Laboratories and Fluka Co., respectively. After careful purification and fractionation, the number-average MW's (M_n) of the HPEO and MHPEO were 4250 and 4700 g/mol, respectively, with near monodisperse MW distributions (polydispersities of 1.03 as measured by gel permeation chromatography with PEO standards). In order to obtain the thin layer samples, PEO/methylene chloride solutions (5×10^{-4} g/mL) were pipetted onto a freshly cleaved mica surface at room temperature; the excess solution was blotted with filter paper. After the solvent was evaporated in an ambient environment, the samples were completely dried in a vacuum oven at 25 °C for several days.

Equipment and Experiments. To measure the thickness of the wetted PEO thin layer on the mica surface, X-ray reflectivity measurements were conducted with a Bruker D8-Advance reflectometer in the theta−theta mode with a horizontal sample stage setup. A Goebel mirror was used to get parallel X-ray beams and to suppress the Cu Kβ radiation. The PEO samples were cast on the mica sheets that were preglued onto a silicon wafer with the sufficiently flat top surface. The sample was then mounted on the heating block of the sample stage, of which the temperature accuracy is ±0.2 °C. After the PEO thin films were completely melted, two experimental temperatures, 74 °C (in the isotropic melt) and 55 °C (in the metastable melt), were used for the X-ray reflectivity measurements.

Using the tapping mode of the in-situ AFM (Nanoscope IIIA with a hot stage), we recorded both the height and phase images during the PEO isothermal crystal growth. The temperature of the AFM hot stage was calibrated using standard materials (benzophenone with a melting temperature (T_m) of 47.9 °C, naphthalene with a T_m of 80.2 °C, and benzoic acid with a T_m of 122.3 °C) to have an accuracy of ±0.2 °C in a temperature region between 40 and 100 °C. The standard materials were first pressed and crystallized into films between two glass cover slides with a thickness of ~1 μm. When the T_m values were approached, the films of these standard materials were heated very slowly on the AFM hot stage by 0.1 °C in every step. The crystal melting of these films was monitored. Since the hot stage was used in a relatively moderate temperature region and the PEO film samples were very thin, the AFM tip effect on film temperature is trivial.[33] Thus, no further calibration on the tip effect was carried out.

During AFM scanning, the cantilever tip-to-sample force needed to be carefully adjusted to avoid height artifacts.[34,35] In particular, care was needed when measuring the depletion zones near the PEO single-crystal growth fronts. On the basis of our experience, the observation of the depletion zone was highly dependent on the experimental conditions. If too many melt droplets set on the pseudo-dewetted thin layer, for example, the depletion zone could not be clearly detected. For the tip-to-sample force, a large force could lead to tip penetrations into the thin wetting layer, resulting in a direct touching of the mica surface. When our AFM experiments were carried out to record the height profile of the depletion zone, we increased the value of r_{sp}, which is the ratio of the set-point amplitude to the driving amplitude, to be the largest; yet, the surface profiles could still be monitored. This led to a disadvantage in that the tip could be easily disengaged with the PEO thin layer surface during the scanning of one image. On the other hand, in order to reveal the single crystals embedded in the melt droplets on the thin wetting layer, we also enlarged the tip-to-sample force to detect the crystals. Because of this, the tip could move the melt droplets and disturb the wetting layer. All the AFM raw data were carefully analyzed without using the planefit procedure. When the crystal growth was not too fast at relatively low ΔT values, a scan rate of 1 Hz and a resolution of 256 × 256 were selected to generate high-quality images; therefore, the time required for every AFM image was ~4.3 min.

After the thin layer samples were completely melted, the PEO isothermal crystal growth from the pseudo-dewetted melt was extremely difficult at T_x values above 30 °C. In order to overcome this difficulty, the self-seeding process[36−39] was performed on the AFM hot stage. After quenching from the melt and crystallizing at $T_x < 30$ °C, the PEO thin layer samples were slowly heated and annealed into the IF(0) crystals. We controlled the temperature to melt most of the IF(0) crystals such that there remained only several IF(0) nuclei embedded in some of the dewetted melt droplets as seeds to initiate the isothermal crystal growth.

Upon the slow AFM heating experiments,[24] we also determined the melting temperature of the IF(0) crystals [$T_m(0)$] for both of the PEO samples. We first grew the IF(0) monolayer single crystals of the HPEO and MHPEO at a sufficiently low ΔT with a prolonged isothermal time. The perfected IF(0) crystals were then heated on the AFM hot stage, and the AFM images were recorded at 0.2 °C temperature increments. Once the IF(0) crystals started to shrink at the periphery, the corresponding temperature was assigned as the $T_m(0)$. The $T_m(0)$ of the HPEO and MHPEO were measured to be 62 and 64.5 °C, respectively, which are the average values over the results of at least five independent measurements. The difference of the $T_m(0)$ values of these two PEO IF(0) crystals is due to the difference in the surface free energies of the crystals caused by different end groups.[40,41]

Results and Discussion

Morphology of the Pseudo-Dewetted PEO Melt. After the PEO samples were heated and melted, the first feature of the PEO thin layer on the hydrophilic mica surface is pseudo-dewetting. Figure 1a shows X-ray reflectivity patterns of the HPEO sample at 74 and 55 °C, respectively. Note that a temperature of 74 °C is well above the $T_m(0)$ of the HPEO at 62 °C. On the other hand, since the sample was completely melted and no seeds were left before the reflectivity measurements, we were able to cool the thin film samples into the metastable state without PEO crystallization at 55 °C. Therefore,

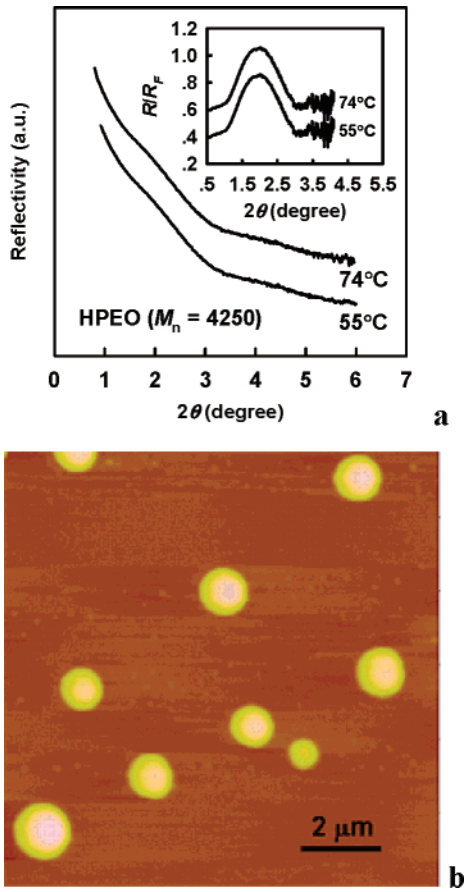

Figure 1. X-ray reflectivity pattern of the molten HPEO monolayer on the freshly cleaved mica surface at 74 and 55 °C (a). The inset of (a) shows the reflection curves normalized by the Fresnel reflectivity, R/R_F. An AFM image of autophobic dewetted molten PEO droplets at 55 °C (b).

the X-ray reflectivity patterns of Figure 1a correspond to the equilibrium and the supercooled melt of the HPEO. In order to clearly illustrate the interference effect, we present in the inset of Figure 1a the reflection curves normalized by the Fresnel reflectivity, R/R_F. At both temperatures, the peaks are centered at $\theta \sim 0.98°$, indicating a continuous layer of the PEO melt with a thickness of ~4.5 nm covering the entire mica surface.[27] This observation agrees with that reported by Reiter and Sommer.[14,15] For the MHPEO, similar X-ray reflectivity patterns were obtained, from which the wetting layer thickness was also measured to be ~4.5 nm. The R_g's of the HPEO and MHPEO samples are estimated to be around 2.5 nm.[43] This indicates that the adsorbed PEO layers on the mica surface may contain one layer of the molten molecules. It is conceivable that the strong interactions of the −OH end groups of the PEO molecules with the hydrophilic mica surface facilitate the PEO adsorption to form the thin wetting layer. For the MHPEO sample, only one −OH end group per molecule is interacting with the surface to form transiently tethered chains on the surface; however, most of the HPEO chains form transient loops due to the interactions from both end groups. We expect that this difference in the interactions will substantially influence the crystal growth behavior of these two samples (see below). However, reasons for the similar thicknesses of these wetting layers in the two PEO samples need to be investigated further.

The excess PEO molecules that do not directly interact with the mica surface may form droplets and sit on the top of the adsorbed layer. Figure 1b is an AFM image which demonstrates the droplet morphology of the pseudo-dewetting melt of the HPEO (similar morphology can be also seen in the figures of AFM images below). It is suggested that the conformation difference between the adsorbed and nonadsorbed molecules may cause the partial dewetting.[31,32] The sizes of the droplets vary with different thermal history applied. Right after the thin layer is melted, the PEO droplets are usually small with the lateral dimension ranging from hundreds of nanometers to a few micrometers and a height of tens of nanometers. With an increase in the holding time at temperatures above the $T_m(0)$, similar to Ostwald ripening, the formation of larger droplets is accompanied by a decrease in and disappearance of the smaller droplets. It should be noted that in this case the segregated droplets are actually connected to each other through the thin wetting layer on the substrate.

Nucleation-Limited (NL) Single-Crystal Growth in MHPEO Pseudo-Dewetted Thin Layers. After self-seeding, the isothermal crystal growth exhibits two stages in the growth process. In the first stage, the crystal growth takes place within the nucleus-containing droplets. Once the molten PEO molecules in the droplet are exhausted, the second stage starts. The crystals continuously increase in their size, accompanied by a shrinking of the neighboring non-nucleus-containing droplets and a decrease in the droplet number. This indicates that not only the droplets which contain nuclei but also those non-nucleus-containing droplets serve as material "reservoirs" from which the molten PEO molecules transport toward the crystal growth fronts. One can expect that the growth in the first-stage should be closer to that in the bulk where the crystal fronts are surrounded by the molten PEO molecules. However, the growth in the second stage requires molecular transport through the thin wetting layer.

Figure 2 shows a set of AFM snapshots at different times in an isothermal crystal growth experiment for the MHPEO sample at a T_x of 62 °C ($\Delta T = 2.5$ °C), which is close to the $T_m(0)$ of the IF(0) single crystal. At this T_x, only the IF(0) single crystal forms with a thickness of 30 nm. Both the first-stage (Figure 2a,b) and the second-stage growths (Figure 2c−f) are observed. The single crystals keep their regularly facetted shape bounded by two (100) and four (120) growth planes.[44] The orientation of two single crystals should be attributed to the orientation of the seeds, which resulted from the self-seeding using a large dendritic crystal as a precursor.[23] We have measured the crystal lateral size change ($2r$ indexed in Figure 2f, which is the growth rate along the [100] direction) as a function of time (t). The plot between the r and t as shown in Figure 3 gives rise to two linear relationships with different slopes, indicating two constant linear growth rates. These two linear growth rates correspond to the two growth stages. The observations of a crystallographically facetted single-crystal shape and the linear growth rates lead to a conclusion that the crystal growths in both stages follow the NL mechanism.

It is specifically interesting that the growth rate in the second stage (4.3×10^{-3} μm/min) is nearly an order of magnitude lower than that in the first stage (2.9×10^{-2} μm/min). On the mica surface, the IF(0) monolayer single crystal with a thickness of 30 nm is much thicker than the wetting layer of ~4.5 nm in the second-stage growth. In the second stage, even assuming that the wetting layer perfectly connects the IF(0) single-crystal growth front, the molten PEO molecules can only access the growth front via the interface, which is only a few nanometers thick. Therefore, the molten PEO molecules must go via the wetting layer near and at the interface. After pushing through the interface, the PEO molecules landed on the crystal growth front, and they needed to climb onto the growth face and extend

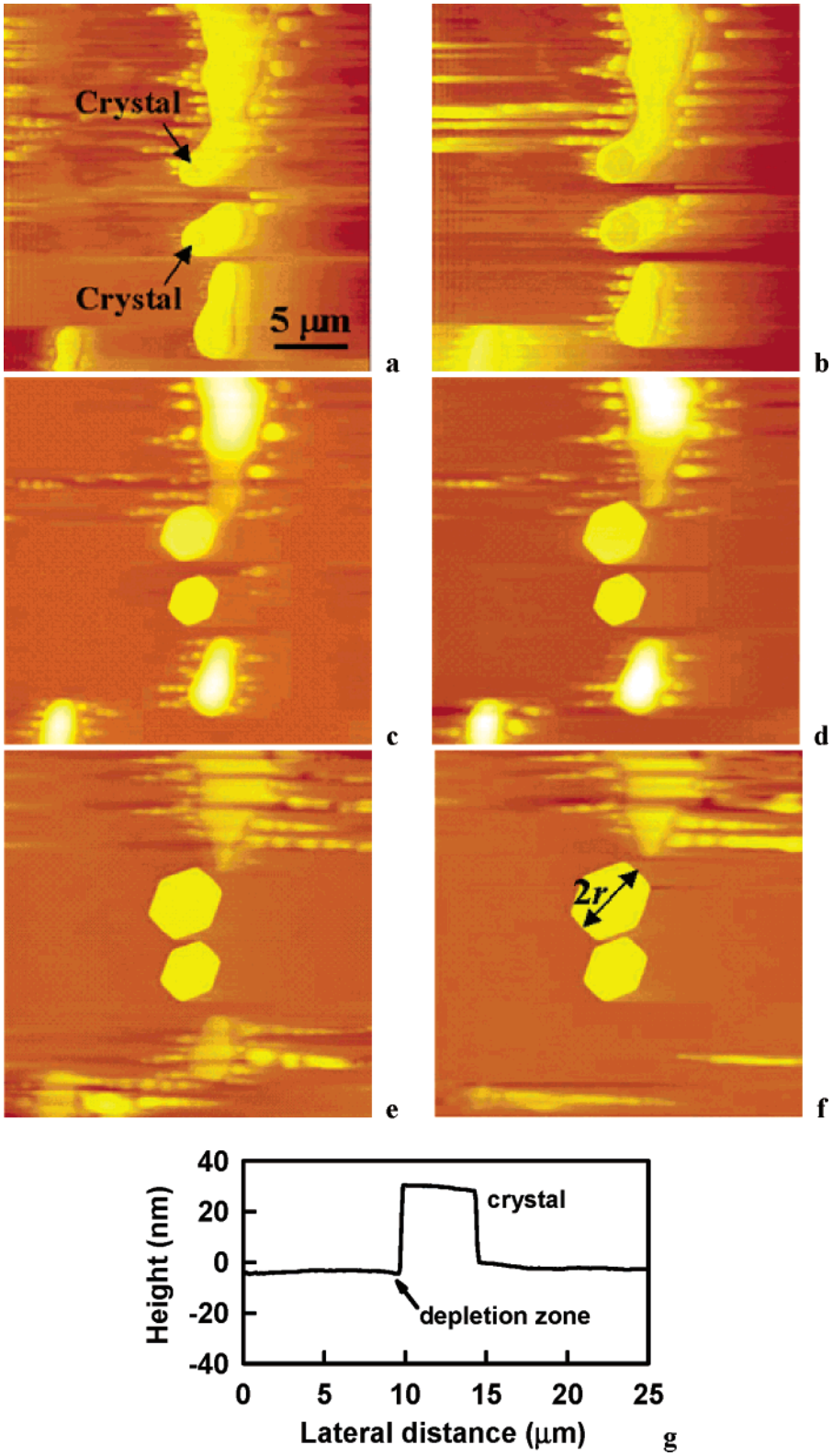

Figure 2. Set of AFM snapshots (a, b: phase images; c−f: height images) for the MHPEO crystallized at 62 °C at different times of (a) 4.3, (b) 21.3, (c) 38.4, (d) 51.2, (e) 119.5, and (f) 187.7 min and (g) a cross-section plot of the depletion zone when the MHPEO sample crystallized at the same T_x.

to the top edge of the lamella via adjusting their conformations. This leads to an increase in the nucleation barrier and a substantial decrease of the growth rate in the second stage. We suggest that the nucleation barrier increase in this stage is largely entropic in nature.

In other cases of thin layer crystallization previously reported,[11−16] the wetting layer thickness near the crystal growth front is thinner than the thickness far away from the interface, inferring the existence of a depletion zone. However, in this case of MHPEO, Figure 2g shows a cross-section plot of Figure 2f, and the depletion zone is not as obvious as in those cases. A specific note should also be put forward for Figure 2. In this series of AFM images, evidence that the AFM tip moves thicker MHPEO melt droplets can be seen. This is due to the fact that

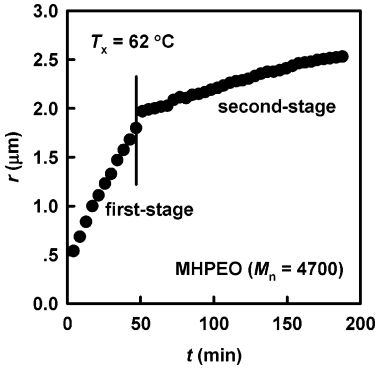

Figure 3. Growing crystal size (r, indexed in Figure 2f) of the MHPEO at 62 °C vs time (t) for the first and second stage of crystal growth.

we utilized a large tip-to-sample force to reveal the crystals embedded in the melt droplets. We wonder whether the tip perturbation could affect the crystal growth.[45] Different tip-to-sample forces were then applied to monitor the second-stage growth. The growth rates observed are very close to those measured using a large tip-to-sample force. We believe that the perturbation to the melting droplets by the tip may relax rapidly and does not significantly affect the crystal growth. Note that MHPEO molecules in these melt droplets will also be transported to crystal growth front via the thin wetting layer. Therefore, although the tip perturbation cannot be completely precluded, the crystal growth rate data measured via the AFM technique provides reliable experimental results for our analyses.

Diffusion-Limited (DL) Single-Crystal Growth in HPEO Pseudo-Dewetted Thin Layers. For the HPEO sample, we have also conducted the isothermal crystal growth experiments. These experiments directly result in the IF(0) crystal with a thickness of 27 nm at ΔT values between 2 and 6 °C. The first-stage growth of the HPEO sample is found to be extremely fast, and our AFM experiments cannot precisely follow the crystal lateral size change with t. We thus focus on the second-stage growth. Different from the facetted MHPEO single crystal shown in Figure 2, the IF(0) single crystals of HPEO always assume more or less round shapes (see Figure 4 at T_x = 57 °C or ΔT = 5 °C). Since the crystals do not have well-defined growth faces or tips, we use the crystal volume (V) as a function of t to monitor the crystal growth. Special attention should be paid in Figure 4e, which is the cross-section plot of Figure 4d. We observe the existence of a depletion zone, although the exact

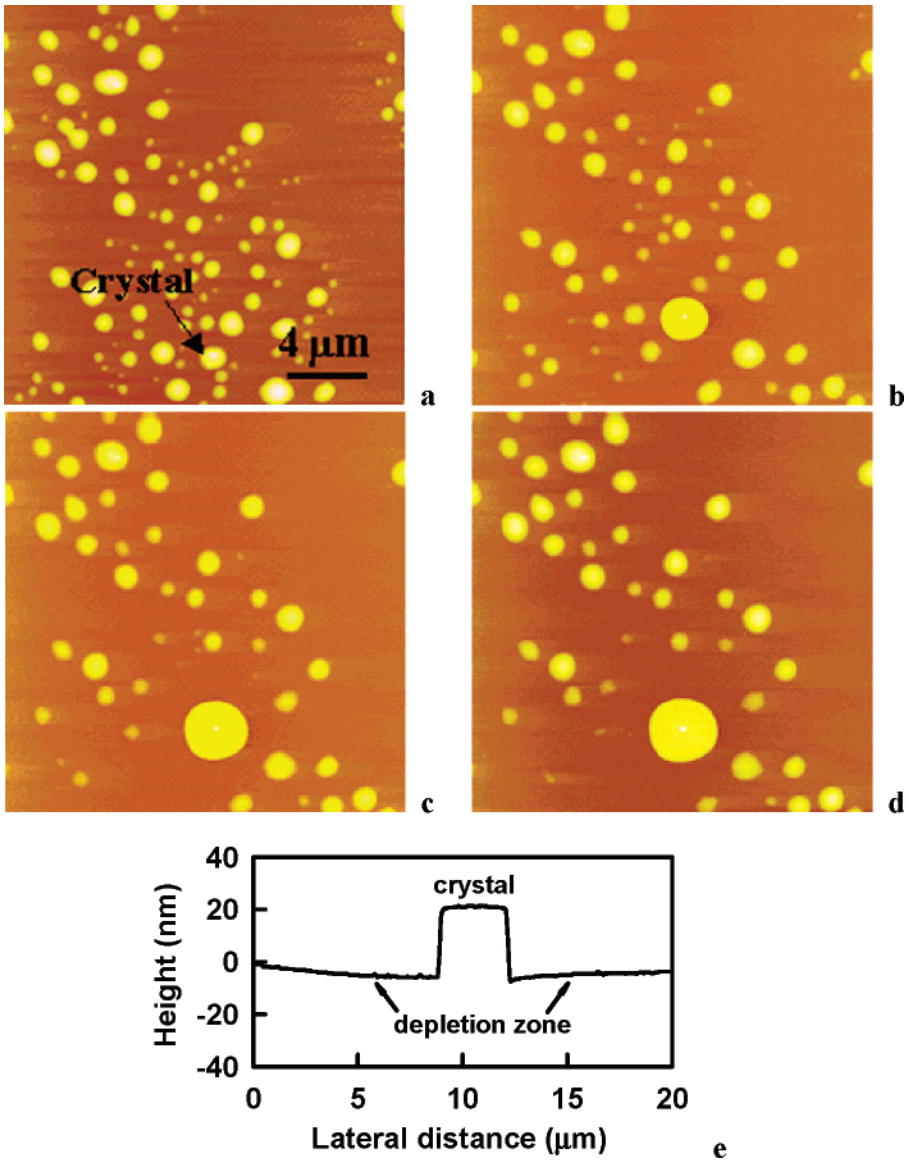

Figure 4. Set of AFM snapshots (height images) for the HPEO crystallized at 57 °C at different times of (a) 8.5, (b) 52.5, (c) 140.8, and (d) 166.4 min and (e) a cross-section plot of the depletion zone when the HPEO sample crystallized at the same T_x.

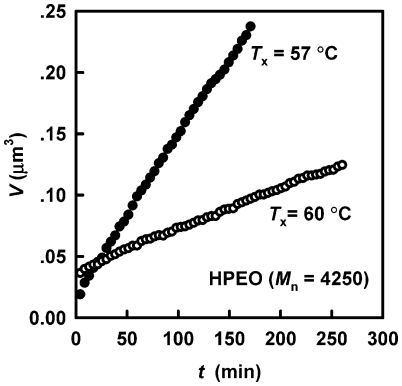

Figure 5. Growing crystal size (V) of the HPEO vs time (t) at T_x of 57 and 60 °C.

profile of this depletion zone cannot be accurately determined by AFM.

In Figure 5, the linear relationship between V and t is particularly interesting. This growth behavior is held for all the isothermal growth of the HPEO crystals in the ΔT region. Since the crystal possesses a constant thickness and identical morphological shape at $\Delta T = 2-6$ °C, the relationship of $V \propto t$ is equivalent to that of the average lateral growth size $r \propto t^{0.5}$, which refers to a DL crystal growth. Note that this relationship of $r \propto t^{0.5}$ may also be observed in other transport limiting processes such as the crystal growth limited by the heat conduction for a polymer crystallized in an injection molding process with transcrystallization. However, in this case, the DL process caused by mass transport is the mechanism for the HPEO crystal growth.

The DL mechanism of polymer crystals with their shapes of fractal dendrites and seaweeds has been reported in the thin layer melt crystallization.[5,11−16,21−25] The observation reported here provides the first experimental evidence for the polymer single-crystal growth which follows the DL mechanism before the morphological instability sets in on a micrometer size scale. Since in the second stage the single-crystal growth from the thin layer melt is sufficiently slow and the latent heat can diffuse away readily, the crystal growth is effectively isothermal. Therefore, the observation of this DL process should arise from a concentration gradient of the transported HPEO molecules, which is related to the depletion zone generated in the front of the HPEO crystals.

Let us define a surface concentration of chains per unit area on the mica surface, C_S. Assuming that the PEO density in the wetting layer is identical to the density of the bulk melt (1.123 g/cm^3), the C_S of the wetting layer with ~4.5 nm thickness should be ~0.7 molecules/nm^2 for the HPEO molecules. This value is much lower than the C_S of 4.7 HPEO molecules/nm^2 calculated in the IF(0) lamellar crystal.[46] When the HPEO molecules' nucleation at the crystal growth front is faster than the molecules transporting to the growth front via diffusion in the thin wetting layer, a depletion zone forms near the crystal growth front. Figure 6a is a schematic sketch of the depletion zone in the crystal growth front. We speculate that specifically in the DL process the wetting layer in the depletion zone may even not be continuous, and the mica surface may not be molecularly covered. Instead, the HPEO molecules within the zone may form a "2D solution". In this sense, the depletion zone can also be considered the precursor of the wetting layer.[47,48] We may use the C_S to describe the diffusion field, which is the lowest at the crystal front and gradually increases until the depletion zone ends at the normal wetting layer (Figure. 6b). With this illustration, the DL process can be understood to

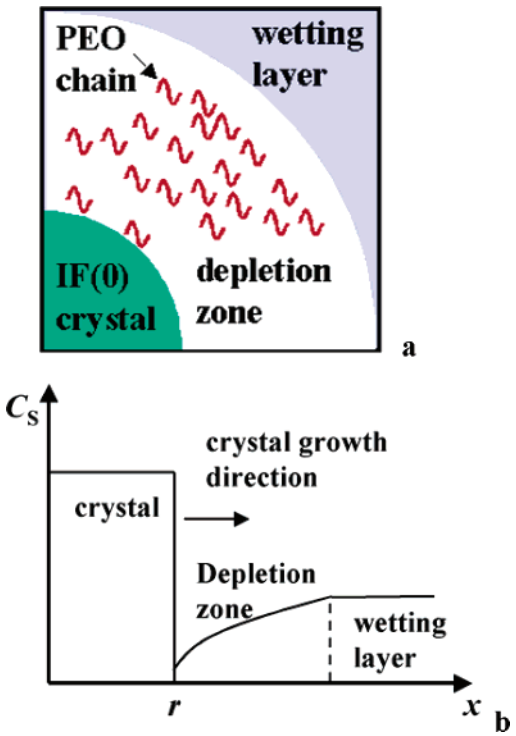

Figure 6. Schematic of the depletion zone between the PEO crystal and the wetting layer (a) and the surface concentration of the PEO molecules (C_S) as a function of distance x along the radial direction from the crystal center (b).

be essentially solution chemical (chemical potential) diffusion controlled.[1] In Figure 5, the growth rate of dV/dt is found to increase with decreasing T_x, which indicates an increase in the concentration gradient. This is due to the fact that as the crystallization driving force increases, the crystal growth at a lower T_x always consumes more HPEO molecules at the front compared with that at a higher T_x within a constant time period. However, at this moment, we cannot precisely measure the thickness change in the depletion zone, and therefore, the explanation provided here remains qualitative.

It is worth noting that at a similar ΔT of ~ 2 °C the MHPEO and HPEO with similar MW's exhibit completely different crystal growth mechanisms. This may be attributed to their different end-group chemistries. For the adsorbed HPEO molecules, both of the −OH end groups in each molecule interact with the hydrophilic mica surface to form a transient loop. However, for the MHPEO molecules, while the −OH end group dynamically tethers on the mica surface, the other hydrophobic $-OCH_3$ end group prefers contacting with the air on the top surface of the wetting layer. It is plausible that the diffusion of the HPEO loops on the mica surface, which needs to have both −OH end groups hopping on the mica surface more or less simultaneously, may be more difficult compared with the diffusion of the tethered MHPEO molecules. Consequently, although the two PEO fractions possess similar surface nucleation rates at the same ΔT, the slower diffusion makes the HPEO crystal growth in the thin wetting layer follow the DL mechanism. However, the quantitative issues still remain for further investigation.

Mechanism Change from NL to DL Single-Crystal Growth in MHPEO Thin Layers. We have also observed that the single-crystal growth of the MHPEO can change its growth mechanism from the NL to the DL process as the ΔT is increased. Figure 7 shows a set of AFM snapshots for the IF(0) crystal of the MHPEO grown at $T_x = 60$ °C ($\Delta T = 4.5$ °C).

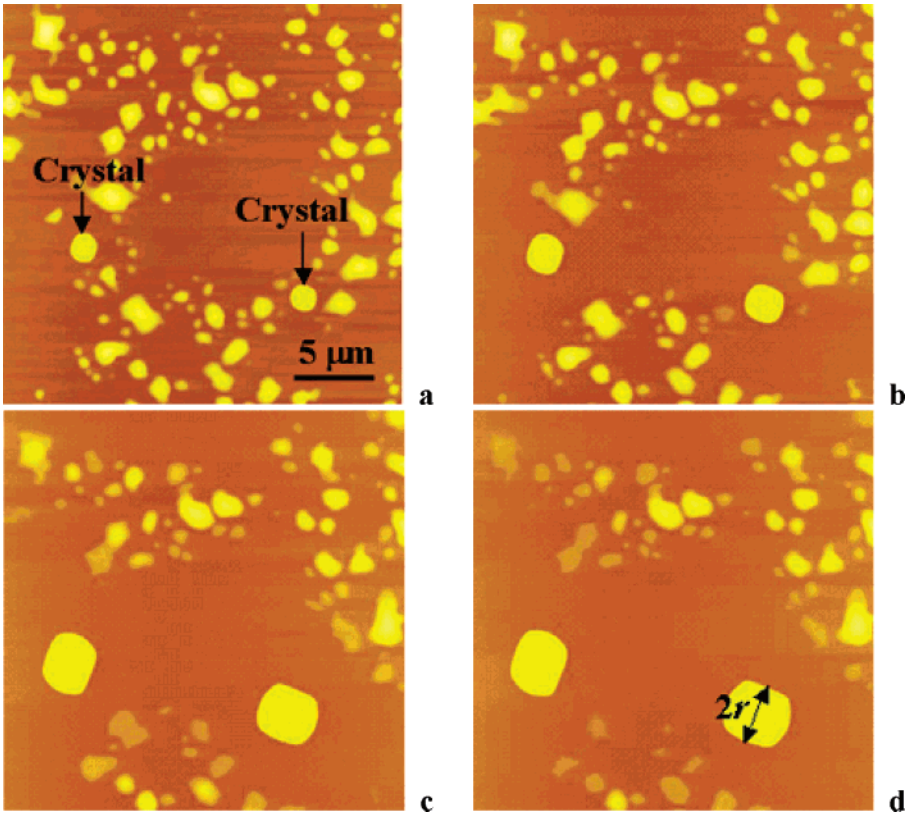

Figure 7. Set of AFM snapshots (height images) for the MHPEO crystallized at 60 °C at different times of (a) 21.5, (b) 64.1, (c) 106.8, and (d) 247.6 min.

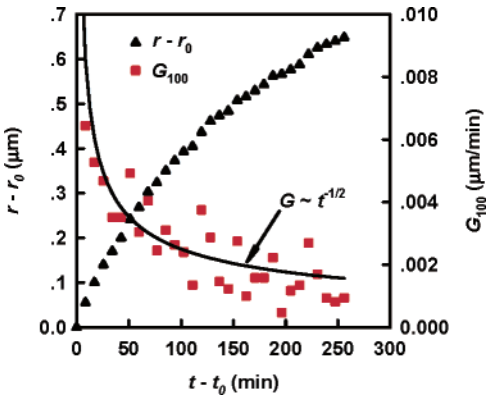

Figure 8. Growing crystal size $r - r_0$ (r, indexed in Figure 7d) of MHPEO at 60 °C vs time $t - t_0$, where t_0 is 21.5 min when the (100) plane can be recognized and r_0 is the half distance between the two (100) planes measured at t_0. The growth rate G_{100} was calculated by $\Delta r/\Delta t$ at time t. The solid line represents the theoretical prediction of $G \sim t^{-0.5}$.

The IF(0) crystals with round shape grow initially, but after 21.5 min, a pair of the (100) planes appears whereas the other growth fronts remain rounded. This morphological evolution is different from those shown in Figure 2 for the same sample crystallized at $T_x = 62$ °C. More importantly, the lateral growth size, r, of the IF(0) crystal is found to be linearly proportional to $t^{0.5}$, indicating that the crystal growth mechanism follows a DL rather than an NL process.

When we analyze the growth rate along the [100] direction, we plot the $r - r_0$ [r is the half distance between the two (100) planes indexed in Figure 7d] and the calculated growth rate, G_{100}, change with $t - t_0$ in Figure 8, where t_0 is chosen to be 21.5 min when the (100) planes can be recognized and r_0 is the size measured at t_0. Although the G_{100} values are relatively scattered, the tendency of the G_{100} decrease with t follows the theoretical prediction of $G \sim t^{-0.5}$ (the solid line in Figure 8). Comparing the AFM results presented in Figure 7 with those in Figure 2, it is intriguing that only a slight decrease of the T_x from 62 to 60 °C can lead to the growth mechanism change from the NL to the DL process. Such a small temperature variation hardly changes the diffusion of the MHPEO molecules. However, the surface nucleation barrier of the MHPEO, which is strongly ΔT-dependent, decreases significantly with increasing ΔT in the temperature range close to $T_m(0)$. This causes the surface nucleation rate to become faster compared with the diffusion rate at $T_x = 60$ °C.

Further increasing the ΔT may lead the MHPEO crystal growth in the pseudo-dewetted thin layers to deeply enter the temperature region controlled by the DL mechanism. In bulk crystallization of the low MW PEO, the lamellar thickness of IF(n) is decreased in discrete steps with decreasing T_x, corresponding to the increase of n.[26−30] This phenomenon is also observed in the PEO crystal growth in the thin layers. For the MHPEO sample, the IF(1) and IF(2) crystals formed at 54 °C $\leq T_x <$ 59 °C and at 42 °C $\leq T_x <$ 54 °C, respectively. We find that the increase of n does not alter the DL mechanism. When ΔT is increased, the surface nucleation barrier correspondingly decreases. This results in the crystal growth fronts becoming increasingly rough so that the crystalline branches start to be generated. Parts a and b of Figure 9 show the AFM images for the IF(1) and IF(2) crystals of the MHPEO crystallized at 55 and 50 °C, respectively. In these AFM images, the center portions of the crystals are the IF(0) crystals as seeds remaining in the melt droplets after the self-seeding process. For crystal growth at these two T_x values, the V of the crystals was found to be linearly proportional to t. As shown in Figure 9a at T_x of 55 °C, some crystals, although they look similar to that in Figure 7, actually have their (100) plane no longer crystallographically flat (pointed by the arrows in Figure 9a as

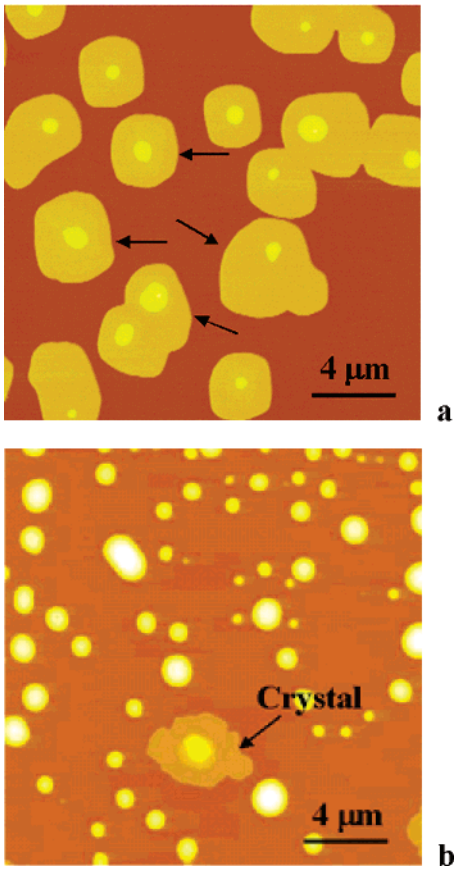

Figure 9. Two AFM images of the MHPEO crystallized at 55 (a) and 50 °C (b), corresponding to the IF(1) and IF(2) crystals, respectively. The arrows in (a) point the curvature on (100) planes.

examples). This implies the birth of morphological instability. At $T_x = 50$ °C, as shown in Figure 9b, the morphological instability becomes evident, wherein the crystal periphery of the IF(2) crystal is branched.

When we further decreased T_x, the MHPEO crystals became fractal dendrites, which could be understood by the DLA mechanism. Similar morphological instability was also observed for the HPEO. With increasing ΔT, the HPEO crystals also gradually lost the round shape and became branched. At T_x below 45 °C, the fractal dendrites become the dominant morphology of the HPEO crystals. For both the MHPEO and HPEO fractions, the branch widths of the fractal dendrites were found to decrease with decreasing T_x.[12,14−16,22,23] Quantitative relationships between the growth rates and branch widths in the two fractions are under current investigation.

Conclusion

In summary, we have used two low-MW PEO fractions with different end-group chemistries (the HPEO has both −OH ends and the MHPEO has one −OH end and one $-OCH_3$ end) as examples to study the single-crystal growth behavior in the pseudo-dewetted thin layer on the hydrophilic mica surface. The purpose of this study is to gain further understanding of the growth mechanisms in thin layers compared with that in the bulk state. Utilizing in-situ AFM equipment in the tapping mode to follow the isothermal crystal growth at different ΔT values, both the NL and the DL processes are experimentally observed. They are identified on the basis of crystal morphologies developed during the single-crystal growth and, more importantly, the relationships between the crystal lateral size and crystallization time. For the NL process, the lateral growth size of the facetted single crystal follows $r \propto t$, whereas for the DL process in this quasi-2D circumstance, the lateral growth size $r \propto t^{0.5}$ ($V \propto t$) when the crystal is more or less round in shape. The changes in the end-group chemistry of the PEO molecules and ΔT have been observed to effectively switch the growth mechanisms between the NL and the DL processes. Because the HPEO molecule has two −OH ends that interact with the hydrophilic mica surface, the retarded diffusion of the molecule through the wetting layer results in the DL process. For the MHPEO sample, the NL process is observed at very low ΔT ($\Delta T < 4$ °C). Increasing ΔT effectively decreases the surface nucleation barrier and thus increases the crystal growth rate, leading to the change from the NL to DL process in crystal growth. Further increasing ΔT does not alter the DL growth mechanism, yet the morphological instability sets in to form branched crystal morphologies.

Acknowledgment. This work was supported by the National Nature Science Foundation of China (NNSFC Grants 20234020, 20025414, and 20374003). S.Z.D.C. acknowledges his support from the US National Science Foundation (DMR-0516602) and ACS acknowledges his support from the Natural Sciences and Engineering Research Council (NSERC) of Canada.

References and Notes

(1) Saito, Y. *Statistical Physics of Crystal Growth*; World Scientific: Singapore, 1996.
(2) Tiller, W. A. *The Science of Crystallization: Macroscopic Phenomena and Defect Generation*; Cambridge University Press: Cambridge, 1991.
(3) Hoffman, J. D.; Miller, R. L. *Polymer* **1997**, *38*, 3151.
(4) Keith, H. D.; Padden, F. J., Jr. *J. Apply. Phys.* **1963**, *34*, 2409.
(5) Lovinger, A. J.; Cais, R. E. *Macromolecules* **1984**, *17*, 1939.
(6) Dukovski, I.; Muthukumar, M. *J. Chem. Phys.* **2003**, *118*, 6648.
(7) Cheng, S. Z. D.; Lotz, B. *Philos. Trans. R. Soc. London A* **2003**, *361*, 517.
(8) Cheng, S. Z. D.; Lotz, B. *Polymer* **2005**, *46*, 8662.
(9) Frank, C. W.; Rao, V.; Despotopoulou, M. M.; Pease, R. F. W.; Hinsberg, W. D.; Miller, R. D.; Rabolt, J. F. *Science* **1996**, *273*, 912.
(10) Reiter, G.; Castelein, G.; Sommer, J.-U. In *Polymer Crystallization*; Reiter, G., Sommer, J.-U., Eds.; Springer: Berlin, 2003; p 131.
(11) Sawamura, S.; Miyaji, H.; Izumi, K.; Suthen, S. J.; Miyamoto, Y. *J. Phys. Soc. Jpn.* **1998**, *67*, 3338.
(12) Taguchi, K.; Miyaji, H.; Izumi, K.; Hoshino, A.; Miyamoto, Y.; Kokawa, R. *Polymer* **2001**, *42*, 7443.
(13) Taguchi, K.; Miyaji, H.; Izumi, K.; Hoshino, A.; Miyamoto, Y.; Kokawa, R. *J. Macromol. Sci., Part B: Phys.* **2002**, *B41*, 1033.
(14) Reiter, G.; Sommer, J.-U. *Phys. Rev. Lett.* **1998**, *80*, 3771.
(15) Reiter, G.; Sommer, J.-U. *J. Chem. Phys.* **2000**, *112*, 4376.
(16) Sommer, J.-U.; Reiter, G. *J. Chem. Phys.* **2000**, *112*, 4384.
(17) Reiter, G.; Castelein, G.; Sommer, J.-U. *Phys. Rev. Lett.* **2001**, *86*, 5916.
(18) Reiter, G. *J. Polym. Sci., Polym. Phys. Ed.* **2003**, *41*, 1869.
(19) Schönherr, H.; Frank, C. W. *Macromolecules* **2003**, *36*, 1188.
(20) Schönherr, H.; Frank, C. W. *Macromolecules* **2003**, *36*, 1199.
(21) Zhai, X. M.; Wang, W.; Ma, Z. P.; Wen, X. J.; Yuan, F.; Tang, X. F.; He, B. L. *Macromolecules* **2005**, *38*, 1717.
(22) Zhai, X. M.; Wang, W.; Zhang, G. L.; He, B. L. *Macromolecules* **2006**, *39*, 324.
(23) Huang, Y.; Liu, X.-B.; Zhang, H.-L.; Zhu, D.-S.; Sun, Y.-J.; Yan, S.-K.; Wang, J.; Chen, X.-F.; Wan. X.-H.; Chen, E.-Q.; Zhou, Q.-F. *Polymer* **2006**, *47*, 1217.
(24) Zhu, D.-S.; Liu, Y.-X.; Shi, A.-C.; Chen, E.-Q. *Polymer* **2006**, *47*, 5239.
(25) Braun, H.-G.; Meyer, E.; Wang, M. In *Polymer Crystallization*; Reiter, G., Sommer, J.-U., Eds.; Springer: Berlin, 2003; p 238.
(26) Arlie, J. P.; Spegt, P.; Skoulios, A. *Makromol. Chem.* **1967**, *104*, 212.
(27) Kovacs, A. J.; Gonthier, A. *Colloid Polym. Sci.* **1972**, *250*, 530.
(28) Kovacs, A. J.; Straupe, C.; Gonthier, A. *J. Polym. Sci., Polym. Symp.* **1977**, *59*, 31.
(29) Cheng, S. Z. D.; Chen, J. *J. Polym. Sci., Polym. Phys. Ed.* **1991**, *29*, 311.
(30) Cheng, S. Z. D.; Zhang, A.; Barley, J. S.; Chen, J.; Habenschuss, A.; Zschack, P. R. *Macromolecules* **1991**, *24*, 3937.
(31) Hare, E. F.; Zisman, W. A. *J. Phys. Chem.* **1955**, *59*, 335.

(32) Israelachvili, J. *Intermoleular and Surface Forces*, 2nd ed.; Academic Press: London, 1991.
(33) Schönherr, H.; Bailey, L. E.; Frank, C. W. *Langmuir.* **2002**, *18*, 490.
(34) Garcia, R.; Perez, B. *Surf. Sci. Rep.* **2002**, *47*, 197.
(35) Ebenstein, Y.; Nahum, E.; Banin, U. *Nano Lett.* **2002**, *2*, 945.
(36) Kovacs, A. J.; Gonthier, A. *Kolloid Z. Z. Polym.* **1972**, *250*, 530.
(37) Chen, W. Y.; Li, C. Y.; Zheng, J. X.; Huang, P.; Zhu, L.; Ge, Q.; Quirk, R. P.; Lotz, B.; Deng, L.; Wu, C.; Thomas, E. L.; Cheng, S. Z. D. *Macromolecules* **2004**, *37*, 5292.
(38) Chen, W. Y.; Zheng, J. X.; Cheng, S. Z. D.; Li, C. Y.; Huang, P.; Zhu, L.; Xiong, H.; Ge, Q.; Guo, Y.; Quirk, R. P.; Lotz, B.; Deng, L.; Wu, C.; Thomas, E. L. *Phys. Rev. Lett.* **2004**, *93*, 028301-1.
(39) Zheng, J. X.; Xiong, H. M.; Chen, W. Y.; Lee, K. M.; Van, Horn, R. M.; Quirk, R. P.; Lotz, B.; Thomas, E. L.; Shi, A. C.; Cheng, S. Z. D. *Macromolecules* **2006**, *39*, 641.
(40) Cheng, S. Z. D.; Chen, J. H.; Zhang, A.-Q.; Heberer, D. P. *J. Polym. Sci., Polym. Phys. Ed.* **1991**, *29*, 299.
(41) Cheng, S. Z. D.; Wu, S. S.; Chen, J. H.; Zhuo, Q. H.; Quirk, R. P.; Von, Meerwall, E. D.; Hsiao, B. S.; Habenschuss, A.; Zschack, P. R. *Macromolecules* **1993**, *26*, 5105.
(42) Zhu, D.-S.; Liu, Y.-X.; Chen, E.-Q.; Li, M.; Cheng, S. Z. D. *Acta Polym. Sinica* **2006**, *9*, 1125.
(43) Fetters, L. T.; Lohse, D. J.; Colby, R. H. In *Physical Properties of Polymers Handbook*; Mark, J. E., Ed.; AIP Press: Woodbury, NY, 1996; Chapter 24. Based on the data reported therein, the end-to-end distance for the PEO with a molecular weight of ~5000 g/mol is calculated to be ~6.3 nm. The radius of gyration is thus estimated to be at around 2.5 nm.
(44) Shcherbina, M. A.; Ungar, G. *Polymer* **2006**, *47*, 5505.
(45) Liu, X. G.; Zhang, Y.; Goswami, D. K.; Okasinski, J. S.; Salaita, K.; Sun, P.; Bedzyk, M. J.; Mirkin, C. A. *Science* **2005**, *307*, 1763.
(46) Takahashi, Y.; Tadokoro, H. *Macromolecules* **1973**, *6*, 672.
(47) de Gennes, P. G. *Rev. Mod. Phys.* **1985**, *57*, 827.
(48) de Gennes, P. G. *Soft Interface*; Cambridge University Press: Cambridge, 1997.

MA062542S